Prototype Design for Grading Structures in Powder Bed Fusion Processes

Maria Mann[1]: Conceptualisation (equal), Investigation (lead), formal analysis (lead), Methodology (lead), Experimentation (lead), Visualisation (equal), Writing original draft (lead), review and editing (equal).

Richard Davies[1]: Resources, review and editing (supporting).

Chris Lawrence[2]: Project administration, Conceptualisation (supporting), Funding acquisition.

O. Ghita[1]: Conceptualisation (equal), Supervision, Visualisation (equal), reviewing and editing (equal).

[1] Centre for Additive Layer Manufacturing, Streatham Campus, Harrison Building, University of Exeter, N Park Road, EX4 4RN, United Kingdom

[2] QinetiQ, Cody Technology Park, Ively Road, Farnborough, GU14 0LX, United Kingdom

Abstract

While targeted alignment in certain Additive Manufacturing (AM) methods such as material extrusion (MEX) and stereolithography (SLA) have been well documented in the research community; a method for targeted alignment of added fillers or fibrous materials in powder bed fusion (PBF) AM devices has yet to be successfully achieved. Similarly, incorporation of multi-materials does not work easily with any of the AM technologies. This study creates a prototype design that could be integrated into a powder bed fusion (PBF) system to allow for multi-material layer deposition and alignment of powders and powder blends. The rheological properties of polyamide powder and a range of polyamide composite blends (incorporating Cf, Gf, PTFE and graphite flakes) in different concentrations were studied and together with the particle size distribution and particle morphology analysis were applied for the design of a prototype hopper for incorporation in the PBF system to create targeted multi-material deposition. Different concept designs, multi-chambered and multi-hopper with hopper angles calculated specifically for the composite blend powders selected were proposed. Initial deposition trials outside a PBF process were tested and the deposited layers measured.

1. Introduction

Since the advent of additive manufacturing (AM), there have been new methods and processes tested that served to improve the printing process, increase the amount and variety of materials that can be used to manufacture, and this new way of manufacturing produced further categories of AM processes to include almost every material, from liquid resins to various polymer filaments, and powdered polymers and metals. Thanks to ongoing research in academia and industry, a once niche and expensive method of manufacturing has expanded to become, more or less, widely accessible across the world. As such, new and burgeoning technologies are continuously being implemented in this industry that are making AM components more reliable, resistant to certain chemicals and environments, and enabling customisation of the materials to make them more suitable to perform under specific conditions.

The addition of spherical and fibrous fillers to improve mechanical properties of polymer materials and to introduce multifunctional characteristics, such as improved thermal and electrical properties, is a process that has been researched and utilised extensively in more traditional methods of polymer manufacturing, such as injection moulding [1-3] and hot press moulding [4-7]. When it comes to AM processes with using two or more filler materials, a goal that research typically focuses on is achieving directional orientation of filler particles and/or fibres. The ability to control the distribution and orientation of fillers creates new possibilities for novel materials with enhanced properties and graded structures to be manufactured. AM technology has the scope to enable users and manufacturers to explore these options.

Though there have been limited attempts to create a method of selective and controlled alignment of fibrous additives and fillers in polymer powders, there have been documented and researched findings of the re-coater process naturally aligning fibrous materials within polymer powder blends in the re-coater direction [8]. Inside the PBF system, during the recoating system the passing blade makes physical contact with longer fibres dispersed within the polyamide powder and align in the direction of movement, while the shorter fibres are dispersed in a more heterogeneous manner. Research carried out by Arai [9] determined that the anisotropic behaviour of glass fibres dispersed in polybutylene terephthalate (PBT) caused increased

tensile strength and modulus of elasticity when measured in the direction of the re-coater, and lowest values in the perpendicular direction. This research was also supported by the findings of Jansson and Pejryd [10], who determined that the orientation of longer carbon fibres combined in with polyamide 12 (PA12) is greater in the direction of the powder re-coater compared to shorter carbon fibres, which tended to orientate more randomly.

Currently the only company that has been successful in achieving multi-layer composite manufacturing is the Aerosint [11]. They have created a system which uses a drum filled with the desired powder material for printing; this is then loaded into a PBF printer and can be controlled in tandem with the standard operations of the printer. This process allows for multi-material selective printing to be carried out inside a PBF system. Though they have had success in printing multi-material metal powders, Aerosint have not researched polymeric materials for their deposition techniques.

Promising research into multi-material processing by laser-based powder bed fusion is also being carried out by a team at the Fraunhofer Research Institution for Casting, Composite and Processing Technology IGCV in Ausburg, Germany [12]. Although the proposed design does not feature a method of filler alignment, it proposes a method of manufacturing graded structures using an integrable multi-material capabilities in PBF systems. Research carried out by Beal et al [13] explored the possibility of using a hopper delivery system that contained a H13 tool steel grade powder and copper powder, as well as combinations of the two powders (up to 50% of each material) to enable multi-material deposition and manufacturing in the x-axis using a high-power fibre-optic delivered Nd: YAG laser. Their results concluded that it is possible to use a hopper powder delivery system and sinter the layers of deposited material to use for additive manufacturing; however, their results uncovered gradient voids in their sintered layers, possibly due to the larger particle sizes of the materials utilised in experimentation. A solution to solving the gradient voids, as provided by Beal et al., is to include finer milled metal powders with smaller particle sizes to fill in the majority of the voids created during deposition.

Therefore, while directed orientation of fibrous filler materials combined and embedded within polymer filaments has been widely explored in MEX [14-43] and in SLA [44-57], selective alignment has yet to be achieved in (PBF) systems. This is a challenge that has been testing both the research and industry fields for many years and, as such, a definitive solution is yet to be readily available.

This paper focuses on presenting findings on PBF processes, focusing on: powder properties, such as the flow and particle morphology, use of fibres or additives, grading of structures, creating multi-materials, and alignment of filler fibres and particles. We also explore the methods that could be implemented for use in PBF systems by examining possible prototype designs for integrated attachment inside a desktop PBF device, the various polymer materials and blends used in PBF systems through experimentation, which include their material properties, examining the factors that are proving to be a challenge for successfully achieving targeted fibre alignment in current PBF technologies, and delivering results and analysis on our experimental work involving the use of a hopper prototype.

2. Proposed Concept Design

This section focuses on the considerations given to the design of a new prototype for use inside PBF, with the ability to grade and align fillers with high aspect ratio.

Several key factors need to be met by the component:

a) The ability to fit and integrate the prototype into a PBF system,
b) to load various types of materials into the hopper,

c) successfully contain the loaded material without inadvertent leaking through the nozzle during handling,
d) maintaining even deposition performance in a high temperature environment,
e) perform in tandem with the PBF printing system.

A desktop powder bed fusion system, SnowWhite manufactured by Sharebot, was chosen to create the prototype system. The spreader blade, which is found in majority of PBF machines and used to distribute powder, has an unused space underneath it that can accommodate the prototype. We illustrate what the design of the prototype would look like in Figure 1 with a custom spreader blade designed based on the original dimensions of the SnowWhite desktop PBF printer.

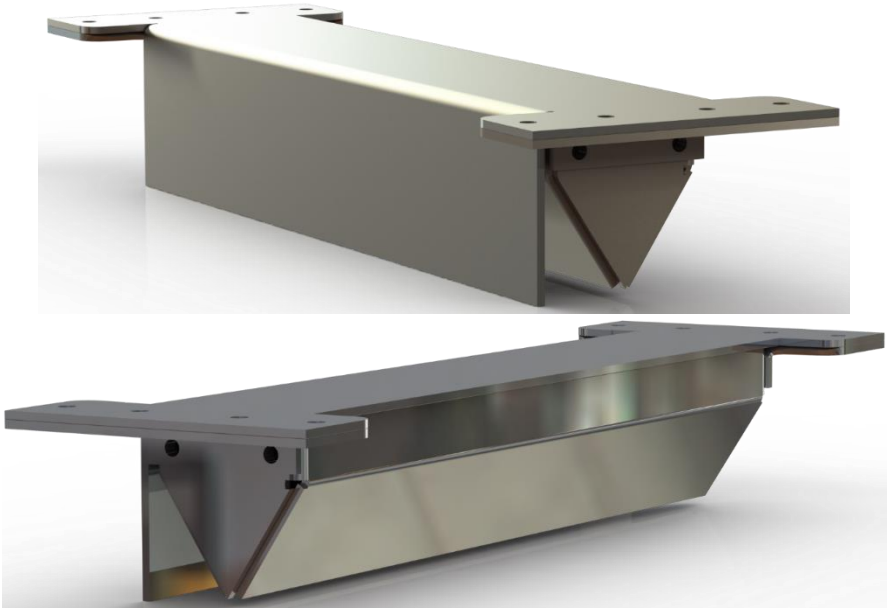

Figure 1 Hopper design in sheet metal, with front and back view, and integrated spreader blade attached.

The spreader attachment within the SnowWhite PBF system is detachable, therefore a design was made for the prototype hopper to be secured behind the blade. This method also opens the possibility for designing blade attachments with the hopper built into the system. A spreading blade is a vital part of any PBF as it evenly distributes fresh powder for additional layers. A small gyroscopic sensor will be attached to the hopper to trigger the activation of the vibration motor during printing, initiating deposition.

Figure 2 illustrates how the prototype will fit inside the printing system.

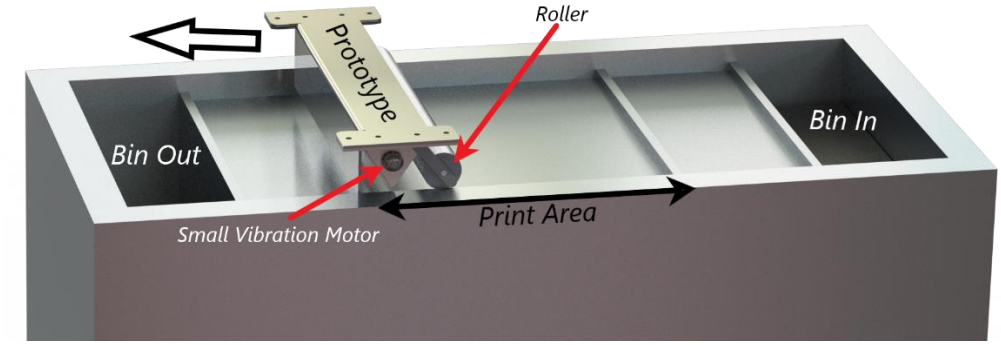

Figure 1 A side image of the hopper prototype as illustrated fitting inside a PBF system. The black arrow represents the direction of movement for the prototype, the hopper has a small vibration motor attached to the outside wall of the hopper.

This design also enables us to create new additions to the system, such as a supplementary spreading blade or roller fitted behind the hopper prototype that will ensure the deposited material is dispersed in an even and homogenous layer before sintering occurs. This blade or roller can also be controlled with the aid of the gyroscopic sensor so that it only lowers when the new material is deposited.

Other designs were considered for the purpose of this research and are illustrated in Figures 3 and 4, though due to time constraints of this project it was decided that the design presented in Figure 1 would be used as the testing bed for future prototypes.

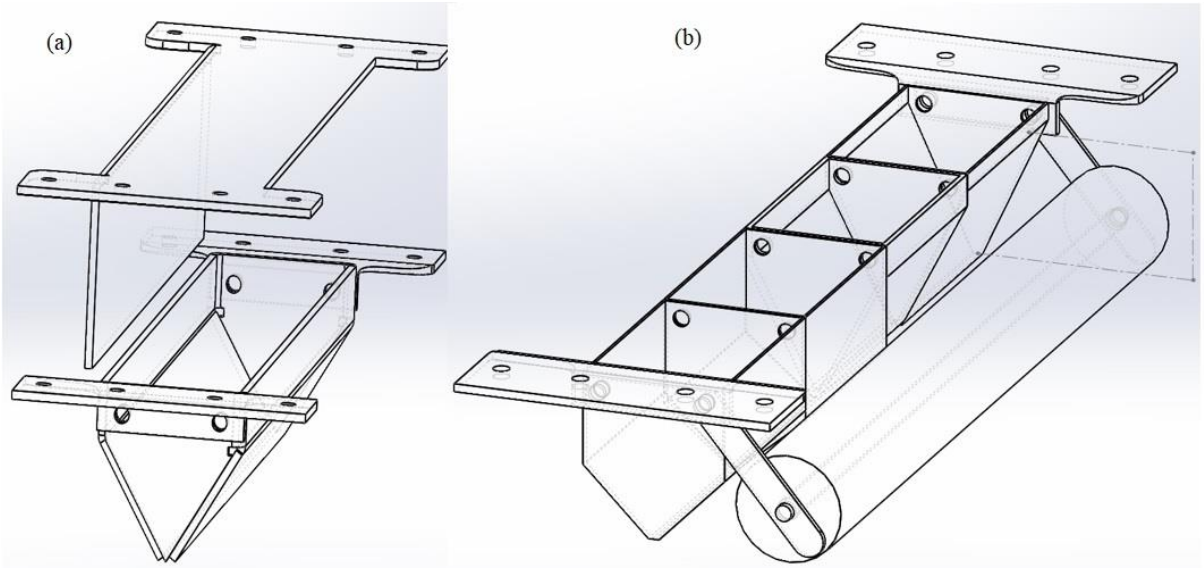

Figure 3 (a) Illustration of the hopper shown in Figure 9 with the hopper and spreader blade detached. (b) Another hopper design with chambers with varying half angles (25, 35, 45, and 50 degrees) to accommodate various powders that require specific half angles to achieve mass flow, with and attached roller to aid in flattening any uneven powder deposition

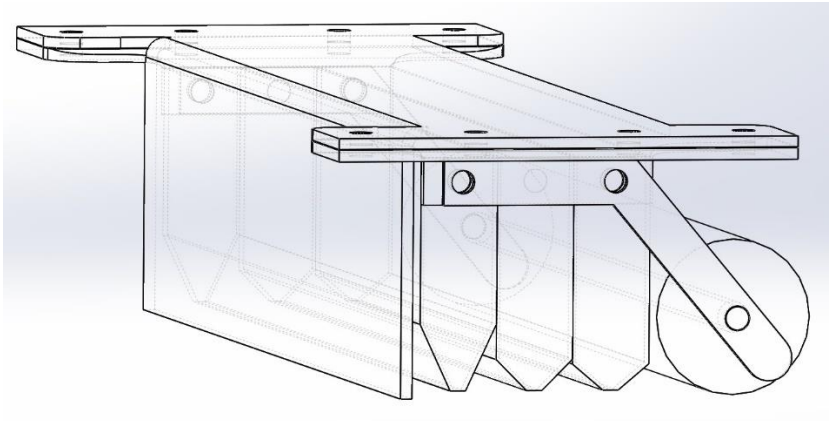

Figure 4 Hopper design with three narrow hoppers attached in a row (35, 45 and 50 degree half angles from left to right)

3.1 Prototype Design Considerations – Theory

Nozzle Size and Geometry

Previous studies [58-60] showed that a hopper with a square nozzle is best suited for depositing a smaller surface area of material. These types of nozzles are best suited for smaller applications and would be complicated to integrate in a PBF system without the use of additional motors and a system control to ensure an even deposition of filler is distributed to create a composite material. A plane flow, chisel and transition hopper all have a longer nozzle profile, which would allow for any powder deposited from this hopper to cover the printing area effectively and therefore it was considered here for further study.

Hopper angle – theory

Several key factors affect powder flow: (i) material properties such as particle size, shape and texture, compressibility, density, aeration, porosity, and potential for charge; (ii) the shape, surface texture of the inner walls, the hopper angle, and aperture geometry.

Figure 5 [66] provides a simple illustration of how the design and nozzle geometry of a hopper dictates how a powder material can be deposited and over how large or small an area, with conical designs having a more concentrated and smaller area of deposition (suitable for more precise depositions) while chisel design offers deposition over a larger surface area.

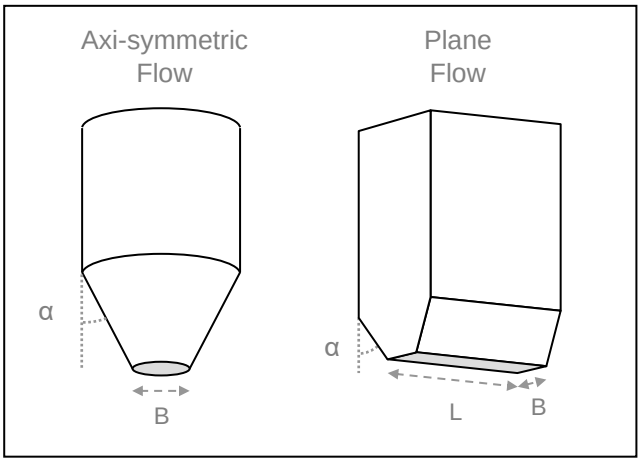

The design of the hopper has a direct effect on the deposition of the powder material as well as the area of deposited material

Figure 6 illustrates the various types of powder flow that can be achieved given the hopper design. Mass flow is typically considered the ideal mode of powder flow as it provides a more consistent, steadier stream of material, and indicates that the full capacity of the vessel can be used. Funnel and expanded flow are less desirable as they create pockets within the powder where the stagnant material is compacted and has the potential to lead to caking, as well as creating erratic flow.

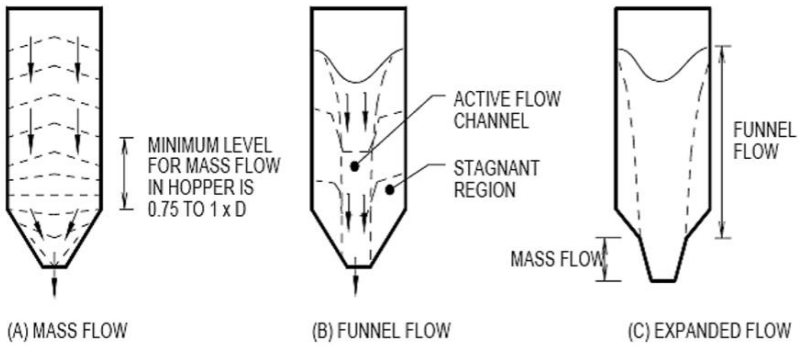

Figure 6 An illustration of mass, funnel, and expanded flow

Figure 7 illustrates how the hopper half angle is taken into consideration when designing a suitable container for a powder material.

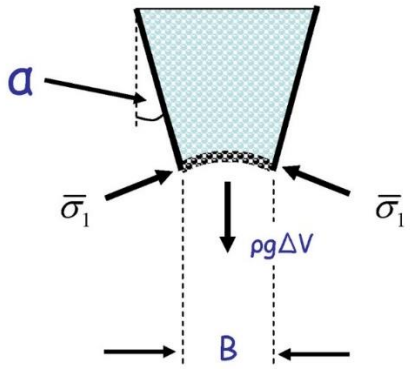

Figure 7 Factors affecting mass flow including hopper half angle [66]

The stress in the arch, $\bar{\sigma}_1$, is a function of both the span and the major consolidation pressure, σ_1. For flow to occur, the stress in the arch must be less than the unconfined yield strength σ_c of the powder. The two criteria for the hopper to operate in mass flow mode are the outlet size (B) and the hopper half angle (α).
With these given factors, the formula for calculating the hopper half angle is given as:

$$\alpha = \frac{\pi}{2} - \frac{1}{2} cos^{-1} \frac{(1-sin\delta)}{2sin\delta} - \beta \qquad \text{Eq. 3.1.1}$$

$$\text{Where } \beta = \frac{1}{2}\{\varphi + sin^{-1} \frac{\sin\varphi}{\sin\delta}\} \qquad \text{Eq. 3.1.2}$$

α represents the hopper half angle, δ is the angle of internal friction, φ is the wall friction angle. With these formulas, a graphical representation of the angle can be created. Along with these mentioned factors, the overall shape of the hopper also has a direct effect on the powder flow properties. Figure 8 shows how the design of the hopper influences mass flow.

In Figure 8, the x-axis shows the allowable hopper angle θ and the y-axis gives the values for the wall friction angle φ. Mass flow is achievable if both θ and φ fall within the limiting mass flow region 1 of the given values. For the chisel design, the length of the hopper must be three times its width to ensure successful mass flow. Problems with powder flow can easily be addressed by simply decreasing the internal wall friction of the container and ensuring the converging walls are steep enough.

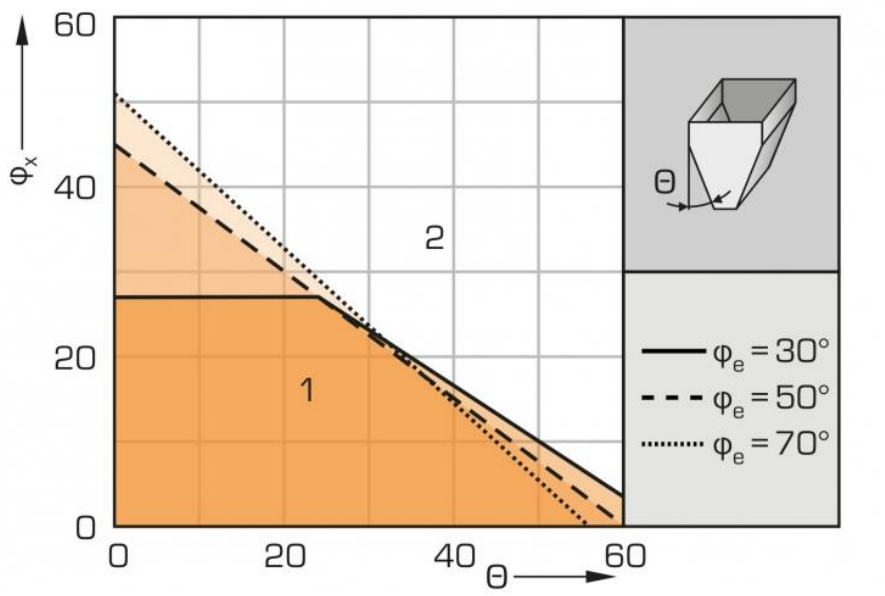

Figure 8 A plot for recommended wall angles for hopper design using a chisel shape [67]

An important factor when a hopper design is being considered is that, for wedge designed hoppers, walled angles are 10-12° less steep than those of conical hoppers. This is because conical hoppers have a smaller nozzle from where the material can flow through, which can in turn affect powder flow, therefore a steeper angle is required to achieve mass flow. Steeper angles, as well as narrow nozzles, mean that there is a constraint in terms of designing a conical hopper to fit inside a PBF system. Also, with the conical hopper design, any changes in powder flow behaviour when introducing various fillers or powder flow enhancers can also change the flow of powder through the nozzle. It is therefore ideal to use a wedge or chisel shaped hopper design if changes to the powder flow behaviour are expected, especially if the powder materials used have high wall friction.

Based on this information and the design parameters for use in PBF systems, it was determined that the wedge design would be ideal to use for our prototype.

Measurements and calculation for the hopper design

Several tests were carried out to determine hopper design, which provides us with the hopper angle to achieve mass flow rate. These experiments included: (a) shear cell test with different rates of shear; (b) wall friction test; and (c) compressibility test.

For the testing required to obtain the hopper angle, all samples were carried out using a Freeman FT4 powder rheometer with the standard procedures provided by the rheometer. Every sample includes a conditioning phase to ensure the powder is free flowing and to eliminate any excess air pockets and ensure a low stress packing state. After conditioning, the appropriate attachment is connected to carry out measurements for shear, wall friction, and compressibility. For shear cell measurements (see Figure 9), a vented piston is used to compress the powder, applying a force of 3kPa to consolidate the powder. The shear stress measurements were collected for 3, 6, and 9 kPa for polyamide powder using the FT4. Shear stress measurements for 3, 6 and 9 kPa were combined to produce the final calculated result for hopper half angle and outlet size.

Figure 9 An image of the shear cell loaded in the FT4 to determine the shear flow of consolidated powder.

Wall friction was carried out which involved the attachment of a steel disk measuring 25mm in diameter at the end of the rod. This test is carried out to measure the wall friction properties of the powder under controlled normal stress. The powder is conditioned and lightly compressed before the steel disk is lowered and pressed to the top surface of the powder. The disk then rotates in a clockwise motion and measurements of the friction between the powder and the steel are measured. This measurement plots the volume change against normal stress and is used to determine whether the powder used is cohesive or non-cohesive. This is a significant step as it determines the behaviour of powder flow. Table 1 presents two repeat measurements (iteration 1&2) and calculated parameters including the hopper half angle for polyamide powder flow through the hopper.

Table 1 Calculated results for plane, or mass flow for our prototype design (δ is the angle of internal friction, φ is the wall friction angle, ρ is the bulk density at σ_1, ff is the flow factor, H(a) the arch thickness variation factor, /σ_1 is the consolidating stress at Arch, α is the hopper half angle and B is the hopper outlet size, or the width of the slot for plane flow vessels)

Plane Flow	δ	φ	ff	H(α)	ρ	/σ_1	α	B
Iteration 1	31.02	12.41	2.36	1.23	0.39	0.13	46.23	0.04
Iteration 2	35.89	12.41	1.84	1.23	0.38	0.11	45.71	0.03

Once the powder flow data for PA12 was determined, it was necessary to determine the hopper half angle that would ensure a good mass flow through the prototype design. The results gathered for the design of the hopper and nozzle were obtained on PA12 powder only as this is the predominant material that has been used during experimentation and the ratio of filler to PA12 will always be low. Through the use of the FT4 equipment, and compiling the rheological measurements collected for each powder tested, it was found that a hopper half angle between 45° and 46° was necessary to achieve effective powder flow for PA12, however it was found that the half angle that could be used for PA12 powder blends that were measured in the FT4 varied significantly. These results are representative solely for PA12 and, as our intention is to combine polyamide powder with a variety of fillers, it was necessary to carry out measurements for all combinations intended for use during experimentation. Table 2 provides the values for hopper angle and outlet/nozzle sizes that have been determined for PA12 powder blends.

Table 2 Hopper angle calculations determined using FT4 equipment for PA12 combined with various concentrations of fillers (glass micro spheres, PTFE powder, graphite flakes, and milled carbon fibre).

PA12 + 10% Glass beads								
Plane Flow	**δ**	**φ**	**ff**	**H(α)**	**ρ**	**/σ_1**	**α**	**B**
Iteration 1	33.35	10.77	2.08	1.24	0.42	0.53	48.42	0.16
Iteration 2	33.44	10.77	2.07	1.24	0.42	0.52	48.4	0.16
PA12 + 20% Glass beads								
Plane Flow	**δ**	**φ**	**ff**	**H(α)**	**ρ**	**/σ_1**	**α**	**B**
Iteration 1	34.43	10.92	1.97	1.24	0.38	0.19	48.06	0.06
Iteration 2	31.84	10.92	2.26	1.24	0.39	0.21	48.39	0.07
PA12 + 30% Glass beads								
Plane Flow	**δ**	**φ**	**ff**	**H(α)**	**ρ**	**/σ_1**	**α**	**B**
Iteration 1	34.05	9.93	2.02	1.25	0.38	0.21	49.58	0.07
Iteration 2	37.27	9.93	1.75	1.25	0.37	0.19	49.48	0.07
PA12 + 10% PTFE								
Plane Flow	**δ**	**φ**	**ff**	**H(α)**	**ρ**	**/σ_1**	**α**	**B**
Iteration 1	36.56	22.64	1.73	1.15	0.65	0.71	30.66	0.13
Iteration 2	43.06	22.64	1.42	1.15	0.64	0.64	30.78	0.12
PA12 + 20% PTFE								
Plane Flow	**δ**	**φ**	**ff**	**H(α)**	**ρ**	**/σ_1**	**α**	**B**
Iteration 1	39.12	18.51	1.6	1.183	0.519	0.037	36.6	0.01
Iteration 2	50.24	18.51	1.234	1.182	0.503	0.029	36.4	0.01
PA12 + 30% PTFE								
Plane Flow	**δ**	**φ**	**ff**	**H(α)**	**ρ**	**/σ_1**	**α**	**B**
Iteration 1	41.27	16.5	1.508	1.197	0.728	0.941	39.4	0.16
Iteration 2	47.86	16.5	1.29	1.196	0.714	0.847	39.2	0.14
PA12 + 10% Graphite Flakes								

Plane Flow	**δ**	**φ**	**ff**	**H(α)**	**ρ**	**/σ_1**	**α**	**B**
Iteration 1	32.84	10.39	2.14	1.245	0.415	0.579	49.1	0.18
Iteration 2	32.41	10.39	2.196	1.246	0.416	0.587	49.1	0.18
				PA12 + 20% Graphite Flakes				
Plane Flow	**δ**	**φ**	**ff**	**H(α)**	**ρ**	**/σ_1**	**α**	**B**
Iteration 1	33.43	10.1	2.082	1.247	0.404	0.313	49.4	0.1
Iteration 2	33.47	10.1	2.077	1.247	0.404	0.312	49.4	0.1
				PA12 + 30% Graphite Flakes				
Plane Flow	**δ**	**φ**	**ff**	**H(α)**	**ρ**	**/σ_1**	**α**	**B**
Iteration 1	35.24	9.51	1.911	1.25	0.634	0.555	50.1	0.11
Iteration 2	38.29	9.51	1.688	1.248	0.629	0.533	49.7	0.11
				PA12 + 10% MCF				
Plane Flow	**δ**	**φ**	**ff**	**H(α)**	**ρ**	**/σ_1**	**α**	**B**
Iteration 1	35.09	17.84	1.86	1.189	-	-0.093	37.7	-
Iteration 2	38.28	17.84	1.648	1.188	-	-0.087	37.6	-
				PA12 + 20% MCF				
Plane Flow	**δ**	**φ**	**ff**	**H(α)**	**ρ**	**/σ_1**	**α**	**B**
Iteration 1	36.33	26.8	1.726	1.123	-	-0.279	24.5	-
Iteration 2	32.16	26.8	2.112	1.122	-	-0.313	24.3	-
				PA12 + 30% MCF				
Plane Flow	**δ**	**φ**	**ff**	**H(α)**	**ρ**	**/σ_1**	**α**	**B**
Iteration 1	37.9	24.62	1.637	1.139	-	-0.491	27.8	-
Iteration 2	44.45	24.62	1.37	1.14	-	-0.456	28.1	-

During shear rheometer measurements of PA12 combined with 10%, 20%, and 30% milled carbon fibre, the rheometer was not able to collect values for bulk density at σ_1 (ρ value) and the values for hopper outlet size (B value). This was due to the "slip" between PA12 particles that milled carbon fibre creates, even in low weight % concentrations, which causes the powder blend particles to shift under the blades off the shear rheometer attachment. Taking into consideration the values for hopper half angle determined for PA12 and PA12 combined with filler, the design was tailored to implement a hopper half angle of 36.2°, which falls within the parameters necessary to achieve plane mass flow for the materials utilised in our experiments. The width of the nozzle was also decreased to 1mm. This is to allow deposition of thinner layers and smaller amount of the material, in a more controlled manner, which is required for optimum sintering conditions.

Materials Selected

The materials that were selected for experimentation include unmodified PA12, milled carbon fibre, PTFE powder, glass microspheres, graphite flakes, as well as combinations of the fillers with PA12 in 10, 20, and 30% weight concentrations.

PTFE powder Zonyl MP1100 was provided by Alfa Chemicals (PSD 4µm) [61], glass microspheres (PSD between 1µm and 40µm) [62] and graphite flakes (PSD +100µm) [63] were obtained from Sigma Aldritch, and milled carbon fibre powder (average fibre length 100µm) was procured from Easy Composites [64].

PA12 was chosen as a base material to test using the prototype as it is a commonly used powder in PBF printing, and it is relatively inexpensive compared to other more specialised options.

The additives have been chosen for the properties they can impart on the material after printing. Milled carbon fibre and graphite flakes are inherently good to use for shielding against electromagnetic interference (EMI), which is one of the key factors in this research. Hollow glass microspheres are a filler that has been used extensively in PBF printing as they offer a multitude of properties, such as a decrease in density, and improved reaction to water exposure and ageing in thermoplastics, depending on how it is used. Hollow glass microspheres can be used on their own to create hollow structures inside the printed part, which has beneficial properties in weight reduction and offers some beneficial mechanical properties such as an increase in the tensile and compressive modulus [65]. This filler can also be modified by using the immersion coating process with conductive or nonconductive metals and polymers.

4. Experimental Methods

4.1 Particle Size Distribution measurements

The particle size distribution and geometry of nylon powder and fillers was carried out using a Microtrac FlowSync particle size and shape analyzer. The system utilises three lasers and a high-speed camera that not only records the size of the powders that it measures, but also includes images of the particles and fibres that have been captured during the measurement, giving a clear representation of the size and geometry. The equipment is ideal for particle analysis as it records the particle geometries of dry powder samples, which eliminates the need for dispersing the material in a solution and potentially causing agglomeration of the sample.

4.2 Powder Rheology

Determining powder rheology is an essential part of understanding powder flow. A Freeman FT4 rheometer was used to measure the powder flow and determine the hopper angle. Powder flow rheology was carried out on materials, which included unmodified PA12, PA12 combined with 10, 20, 30% milled carbon fibres (MCF), PA12 combined with 10, 20, 30% glass microspheres, PA12 combined with 10, 20, 30% graphite flakes, PA12 combined with 10, 20, 30% milled PTFE powder.

The FT4 recorded a series of measurements, also referred to as test numbers (11 in total for each sample), with a pre-set value of varying tip speeds (-100, -70, -40 and -10 mm/s) to determine the total energy in mJ. The measurement characteristics carried out for shear properties, including shear cell and wall friction, are described in section 3.1.

Results are provided for BFE, SI, FRI, SE and CBD by the FT4. BFE is the energy that is required to displace a constant volume of conditioned powder using a specific flow pattern and rate. SI refers to the ratio between test samples where stable powder has a value of 1. FRI measures changes in BFE when the flow rate of a standard test is reduced by a factor of 10; this means that powders with a high value are more difficult to process than those with lower values due to their flow energies and behaviour being variable. The BFE measurement is obtained by the FT4 rheometer when the spiral blade moves down and into the powder, displacing it as it rotates. These values tend to be indicative of flow behaviour under moderate

to high stresses and confined conditions. Specific energy (SE) is a value obtained when the spiral blade moves up and through the powder sample in a way that gently displaces the material and CBD is the recorded density of the measured powders.

4.3 Configuration Set Up for Powder Deposition Testing

To carry out the powder deposition experiments using the prototype hopper design in a way that would replicate the motions inside a PBF system, a repurposed bed from an in-house built FDM printer was utilised. The printhead of the system was removed, leaving the Z-axis free to attach the prototype design onto.

To obtain information on the weight and height of deposited material, the prototype was loaded with powder material of unmodified PA12 and filler combinations and deposition was carried out onto the print bed. 3000mm/min to 1000mm/min print bed speeds were used in 500mm/min increments to determine the effect on weight and height.

For all variants of the powder combinations, between 10 and 12 grams was loaded into the prototypes with 1mm nozzle width. The vibration motor was attached to the outside wall of the hopper in a centralised position to allow even deposition of powder. Using a standard size microscope slide with a strip of double-sided 3M tape running the length of the slide, the slide was weighed on a scale and the values recorded before removing the cover of the double-sided tape and placing the slide on the print bed underneath the hopper. The tape was used to better adhere the powder and prevent shifting during handling. Once the slide was properly aligned in a central location relative to the nozzle with 1cm gap in the front, the bed speed was entered, and movement initiated in tandem with the vibration motor.

4.4 Determining thickness and weight of deposited materials

Once the powder was completely deposited onto the entire length of the slide, it was carefully moved to the scale and the weight recorded. To determine the height of the deposition, every slide was placed on the base of a Taylor Hobson Talyscan 150 laser interferometer. The height of the equipment was calibrated respective to the sample being measured and a speed between 100µm and 150 µm per second was selected for measurement. The direction of measurement was set in the x-axis, with a 2-3cm distance of total measurement taken that was recorded where the starting point was marked at a section of the glass slide with no deposited powder. After completion, the sample was removed and the laser and bed of the Talyscan reset to zero so the measurements could be repeated for other samples.

5. Results and discussion

5.1 Particle Size Analysis

Particle size is significant as it can influence how the material behaves when combined with other powders. This section focuses on the analysis of particle size distribution measurements. Table 3 provides the cumulative values collected for D10, D50 and D90 and Figure 10 provides the plotted particle sizes of all powders, excluding blends, used in our experimentations.

Table 3 Particle size distribution with values collected for D10, D50, and D90

	Materials				
Particle Size Distribution	*PA12*	*Milled Carbon Fibre*	*Glass Micro Spheres*	*PTFE powder*	*Graphite Flakes*
D10	21.57	9.2	11.21	28.8	95.3
D50	46.66	22.45	29.79	82.05	178.5
D90	76.8	98.17	182.1	820	265.4

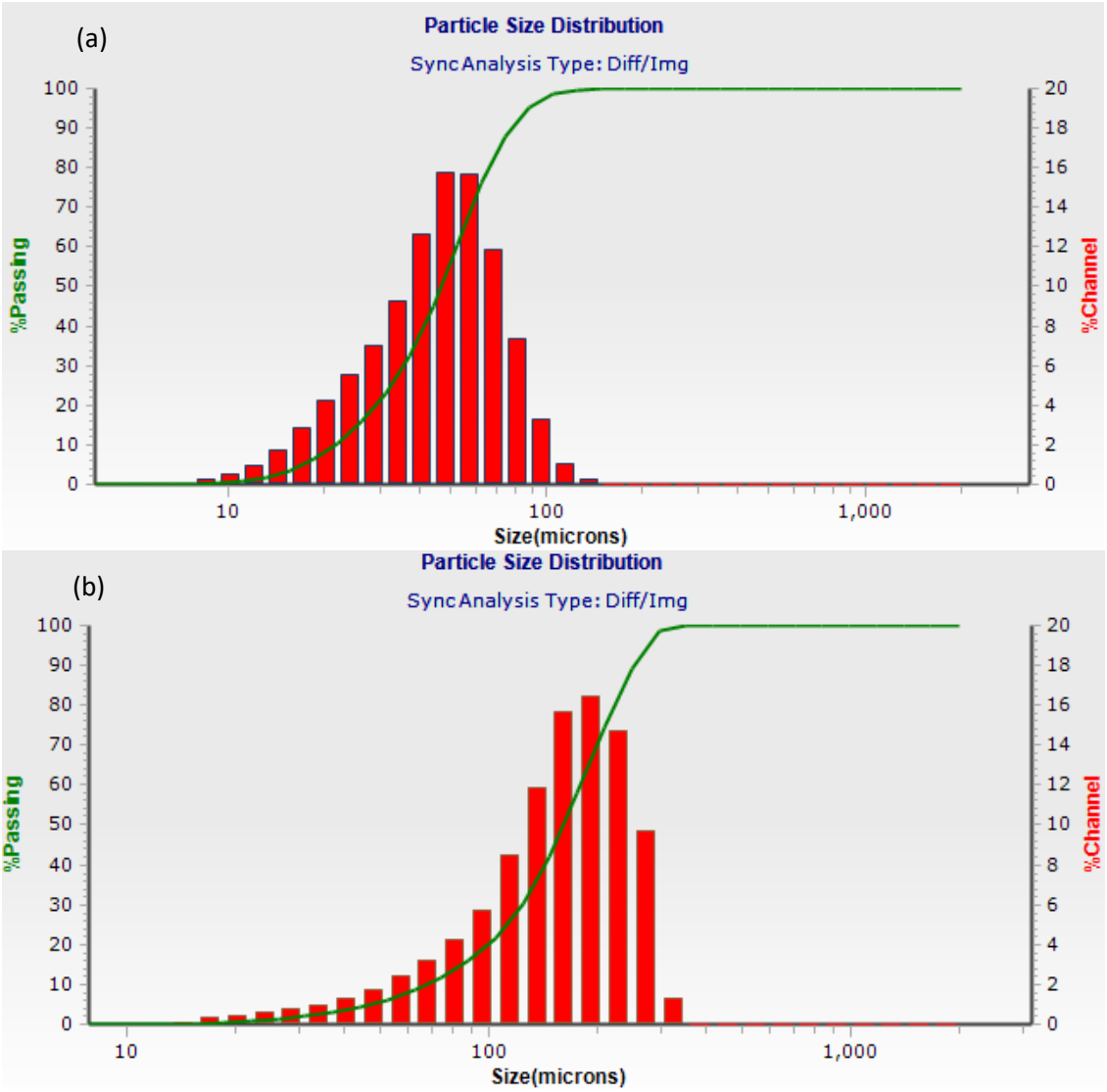

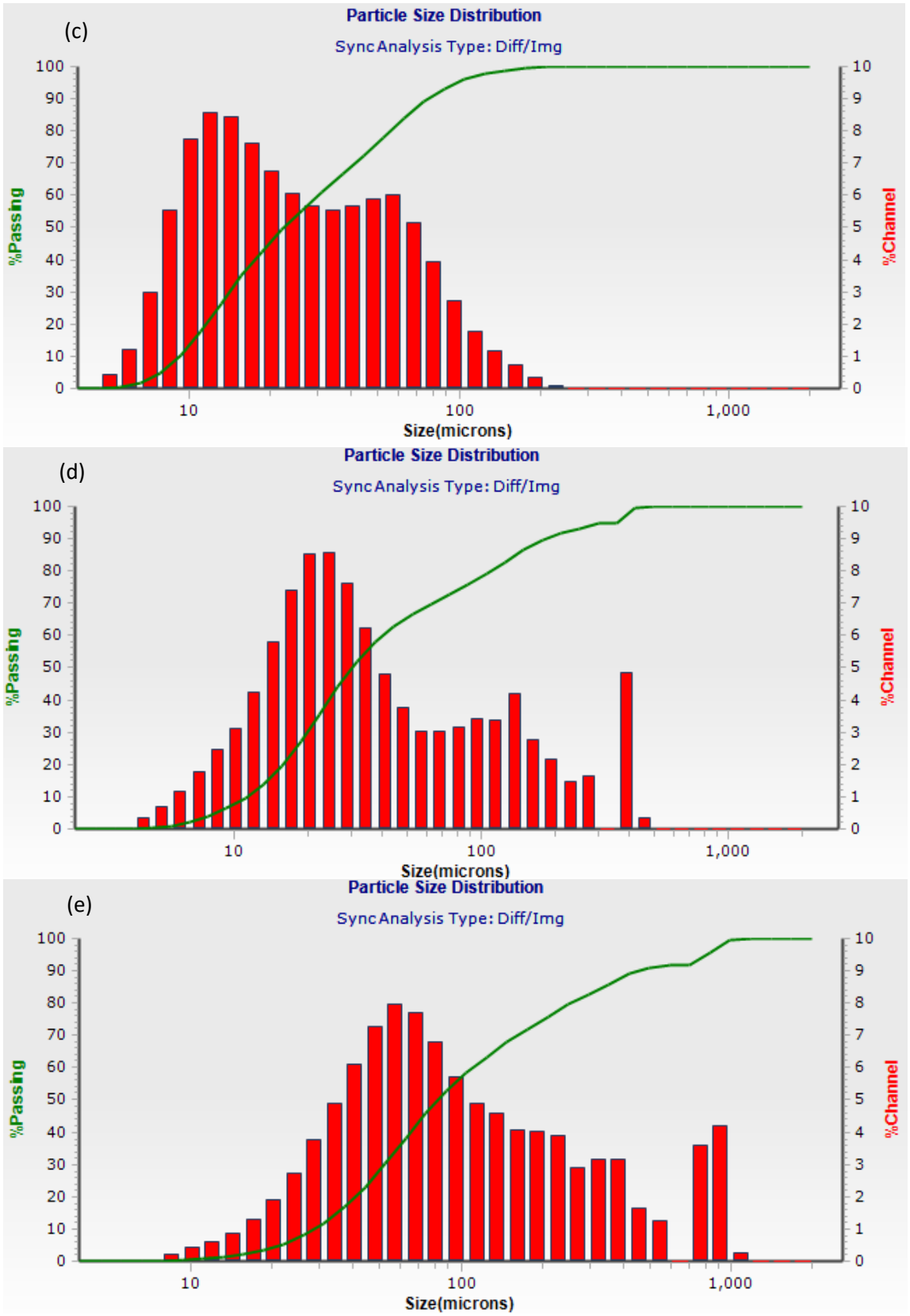

Figure 10 Particle size results for (a) PA12, (b) graphite flakes (c) milled CF (d) glass microspheres (e) Zonyl PTFE powder

95% of the milled carbon fibre that has been used throughout our experimentation has been shown to fall within the 95µm size and examination of the images captured on the Microtrac has shown the fibres are uniform in their form with no abnormalities such as possible contaminants attached to their surfaces or irregular shapes to the fibres.

For polyamide, the results from the particle analyser show that the range of particle sizes is characteristic for the material, even when compared with results gathered during our research. This makes polyamide an ideal powder material to use for our deposition trials, and because various other filler materials can be safely combined together.

Compared to particle size distribution measured for polyamide and milled carbon fibre, the graphite flakes are larger. Although these values appear significant, they are the measurements taken of the flakes at their widest points. The thickness of the flakes themselves is quite low and therefore does not pose an issue for deposition through our prototype design. Overall, the graphite flakes are of a reasonable size and, during deposition trials, have not shown to cause any problems in the mass flow of the powder, such as causing agglomerations or disruption to the powder flow.

The particle size measurements taken for PTFE powder, displayed in Figure 10 (b), have shown to have the highest particle size of all samples analysed. Our results are divergent to the manufacturer's own particle size measurements, which were detailed as having an average particle size of 4µm. One explanation for the high particle size measurement that has been recorded in our tests is that, over time, the powder has agglomerated slightly. PTFE is a soft material and, if the material is left to sit for extended duration without agitation, the particles begin to compact and adhere together , forming larger particles as we see in these results. This might be mitigated in the future if the material is agitated and passed through a series of fine meshes to break apart the agglomerates. However, these larger particle sizes can directly affect the overall layer thickness of deposited material, which needs to be at or below 100µm in order to sinter effectively in the PBF system without creating pockets of un-sintered powder, uneven surface textures and delamination.

Particle size measurements carried out for glass micro spheres are illustrated in Figure 10 (e). Results show that there are some larger particles that have been recorded during the measurements. Typical particle size measurements for glass micro spheres normally ranges below 100µm. At D90, the particle measurements were recorded as 182.1µm, which is higher than the average size for glass micro spheres. It is possible that agglomerates of spheres have formed over time, as the powder remains stagnant for extended periods of time in its storage container. This matter can also be remedied with the use of fine mesh sieves to eliminate unwanted larger particles Despite the high value at D90, D50 was recorded at 29.79µm and D10 at 11.21µm, which means that there is a range of particle sizes for the glass micro spheres filler that would allow for effective deposition through the hopper nozzle.

5.2 Powder Rheology

Powder flow characteristics, which include basic flowability energy (BFI), stability index (SI), flow rate index (FRI), specific energy, (SE), and density of the materials tested, were measuring using the FT4 powder rheometer and the values are displayed in Figure 11 and Table 4.

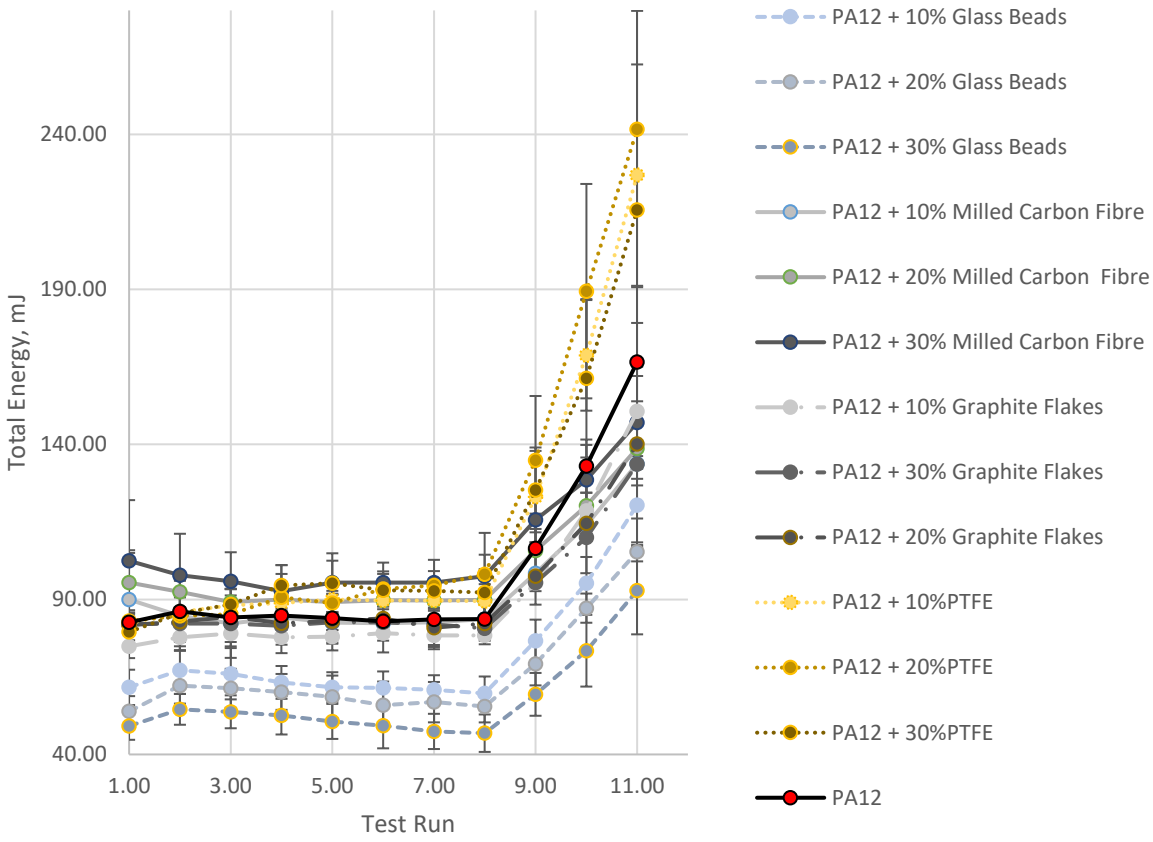

Figure 11 Powder flow rheology recorded using FT4 rheometer for PA12 and PA12 combined with varying concentrations of fillers by wt%. Total energy represents the torque and vertical force signals, which is the energy that is required to move the rotating blade through the powder from the top of the powder column to the bottom.

Table 4 Powder Flow results obtained using the FT4

Material and blends	BFE, mJ	SI	FRI	SE, mJ/g	Total Energy Standard Deviation
PA 12 plain	75.1	1.01	2.14	6.16	8.2
PA12 + 10%Glass beads	59.1	0.99	1.86	5.09	25.5
PA12 + 20%Glass beads	49.3	1.01	2.05	4.92	10.2
PA12 + 30% Glass beads	42	0.91	1.85	4.73	64.6
PA12 + 10%MCF	75.5	1.05	1.55	5.80	26.5
PA12 + 20%MCF	86.5	1.02	1.54	5.76	29.7
PA12 + 30%MCF	87.1	1.08	1.44	5.93	23.8
PA12 + 10%Graphite Flakes	74.1	1.05	1.73	5.44	23.4
PA12 + 20%Graphite Flakes	78.	1.01	1.70	5.69	29.8

PA12 + 30%Graphite Flakes	861	0.99	1.66	5.32	15.6
PA12 + 10%PTFE Powder	91.4	1.07	2.72	8.31	90.6
PA12 + 20%PTFE Powder	97.1	1.19	2.91	8.60	25.8
PA12 + 30%PTFE Powder	98.72	1.18	2.93	8.44	16.5

From the results illustrated in Figure 11 and Table 4, the variation in different fillers impacts these properties is visible.

For the majority of the fillers used in the experiments, even in higher concentrations, the flowability of the materials does not seem to be impacted greatly; in fact, the addition of graphite flakes, glass micro spheres and milled carbon fibre appears not to negatively influence the properties of PA12. A slight reduction in the SI values for PA12+10%Glass beads, PA12+30%Glass beads, and PA12+30%Graphite flakes. The addition of glass beads clearly has an effect on BFE. This is due to the nature of glass micro spheres being an inherently smoother filler material compared to others used that prevents PA12 from affixing to itself, which can have the added advantage of preventing agglomeration.

From the results in Table 4, we observe all the values recorded for BFE, SI, FRI, SE, and CBD (density). The majority of the PA12 and filler combinations are stable, having consistent values for BFE, SI, FRI and SE; however, when PA12 is combined with PTFE powder these values increase, indicating that flowability of the powder mix is less stable compared to the other combinations. This is due to the higher density and pliable nature of PTFE powder, which is much softer compared to PA12 and when heavily mixed, compressed or agitated, the powdered PTFE agglomerates and poses a challenge for deposition. This conclusion is supported by the BFE values in Table 4, as higher BFE values indicate the presence of denser, larger, and more adhesive particulates, and during measurements this results in a lower screw speed in the FT4 system as the spindle requires higher energy to displace the powder. This might be mitigated with the addition of powder flow agents, which are typically glassy oxides, metallic stearates, fumed silica, or fluoroplastics, which improve overall powder flow and behaviour by reducing the contact area between larger particles. The combination of PA12 with hollow glass beads has the opposite effect for density and BFE values, which is to be expected as hollow glass beads have an overall lower density to PA12. Consequently, this results in less energy required to displace the powder, as indicated by considerably lower BFE values when compared to all other fillers used and the control sample.

In the data presented in Table 4, the standard deviation values for PA12 plain and PA12 + 10%MCF are considerably higher compared to other powder combinations. This is possibly due to PA12 absorbing moisture during use and handling, which can influence the flow of powder.

Despite the higher concentration of PTFE filler to PA12 powder, deposition trials were successful and there were no observable instances of powder agglomeration; in fact, the observed powder flow through the 1mm nozzle prototype was better for PA12 combined with PTFE than with glass micro spheres, which at higher concentrations physically hindered powder deposition due to formation of stagnation points within the hopper prototype.

5.3 Deposition Trials

This section focuses on the deposition results obtained using the chisel design with 1mm nozzle width, as well as the results from the filler alignment experimentation that was carried out.

5.3.1 Powder Combinations and the Effects of Varying Fillers

One of the considerations that required addressing during the experimentations were what effects varying concentrations had on the overall filler distribution in the powder, if it affected layer thickness, and whether the addition of fillers improved or hindered deposition. Figure 12 illustrates two deposition trials that were carried out using unmodified PA12 and PA12 combined with 30% concentration of milled carbon fibres.

Figure 12. Deposition trial using PA12 combined with 30% milled carbon fibre (left) and unmodified PA12 (right)

It was found that the combination of PA12 with fibrous filler produced a more floccose surface texture when compared with the deposition of the unmodified PA12. This was due to the fibres that displace the PA12 powder once deposited and create a surface texture that appears softer. The slightly uneven surface texture was caused by the movement of the stepper motors in the printbed used for deposition trials. As stepper motors are commonly used in PBF systems for the spreading blade, a similar result will be encountered once the testing phase moves to a desktop PBF system; however, this uneven texture can be easily mitigated with the attachment of a roller mounted behind the hopper that will lightly press down on the freshly deposited powder. This solves the issue with the slightly wavy surface texture and can aid in filler alignment.

5.3.2 Varying Speed of Deposition on Layer Thickness and Weight

A significant factor that affects the weight and height of deposition is the speed with which the prototype moves across a surface. Figure 13 illustrates a measurement of the height of PA12 powder deposited through the hopper prototype with the print bed moving at a speed of 3000mm/min. To effectively determine the thickness of deposited powder as well as the surface profile, Talyscan surface profiler was used on powder deposited onto glass microscope slides.

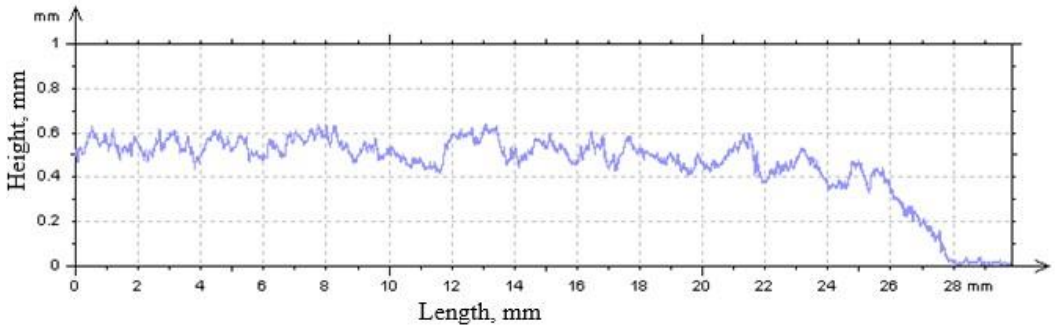

Figure 13 Talyscan image displaying the height measurement taken for PA12 deposited onto a microscope glass slide at a bed speed of 3000mm/min

Figures 14 and 15 present the results that have been collated from a series of deposition trials with PA12 and PA12 combined with milled carbon fibre that highlight the effect of speed versus height and weight of deposited material.

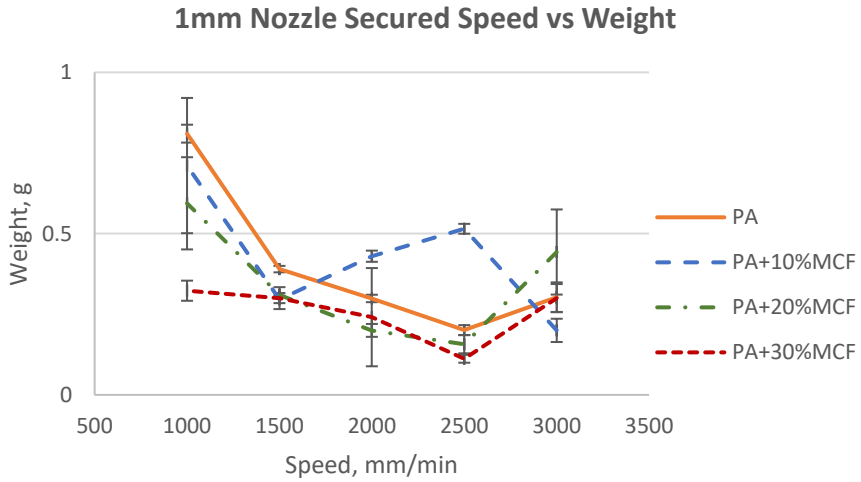

Figure 14 Speed vs weight measurements for prototype with a 1mm wide nozzle

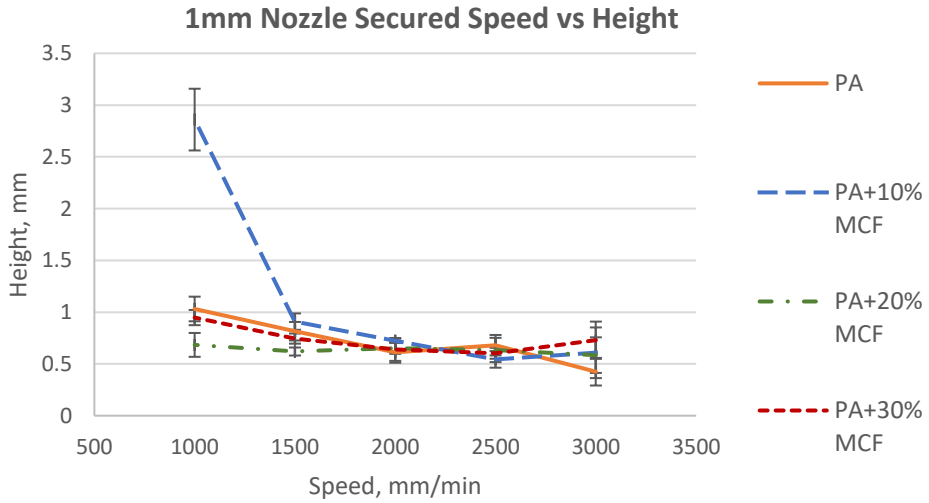

Figure 15 The speed vs average layer height deposition results collected for PA12 and PA12 filler combinations using Talyscan white light interferometry.

Higher print bed speeds (3000mm/min) resulted in lower weights recorded for all samples compared to lower speeds (1000mm/min). This also translated to lower cross-sectional profile values for the samples deposited at 3000mm/min compared to 1000mm/min; therefore higher bed speeds result in thinner cross-sectional profiles of materials.

In Figure 14, a higher concentration of milled carbon fibre to PA12 results in overall less material deposited on the substrate. This can be attributed to the fibrous filler which has a lower density and weight to PA12, thus PA12 combined with higher concentrations of low-density filler can result in the deposition of material with lower weights recorded. Each measurement was carried out five times for every powder combination.

The surface profile analysis and cross-sectional heights are significant values to consider for successful powder deposition that could be sintered inside a PBF system. Our goal is to achieve sub 100µm layer thicknesses. Figure 15 illustrates the height deposition achieved using the chisel design prototype with variations in milled carbon fibre concentrations combined with PA12 powder. After initial experimentations carried out with the milled carbon fibre filler, other filler materials were incorporated with PA12 in 10, 20, and 30% concentrations to explore the effects having various fillers has on layer heights. Once initial deposition experiments were carried out for PA12 and PA12 combined with milled carbon fibre, other fillers were combined with PA12 in similar weight percentages to observe effects on layer height and the weight of deposited matter.

Figure 16 shows the calculated average layer height values that have been recorded for PA12 and PA12 combined with various concentrations of glass micro spheres, milled carbon fibre, PTFE, and graphite flakes. The calculated average layer height values were obtained using known values for the volume of the glass microscope slide and weight of deposited material. Values were collected for print bed speeds at 3000mm/min. This speed was chosen to represent the results as it is a similar speed with which the spreading blade moves inside PBF systems. PA12 combined with varying concentrations of fillers show how the different concentrations can affect the height of deposited layers. We can observe that a higher concentration of filler has a higher probability of creating a thinner layer deposition; although, there are some exceptions to this, as is noticeable with PA12 combined with 20% and 30% milled carbon fibre. This is due to the larger size and elongated geometry of milled carbon fibre compared to PA12 particles, which when combined in higher concentrations tends to create slightly raised structures once the material is deposited. Observing the deposited PA12 combined with 30wt% of milled carbon fibre through an optical microscope, it was found that the orientation of the fibres is heterogeneous, with fibres aligned randomly in the x and y directions. This result was determined to be due to the short length of the milled carbon fibres as they are approximately 100µm in length and smaller; therefore, longer fibrous additives are required to achieve the desired alignment in the x or y direction during the deposition process as they are easier to physically manipulate and orientate.

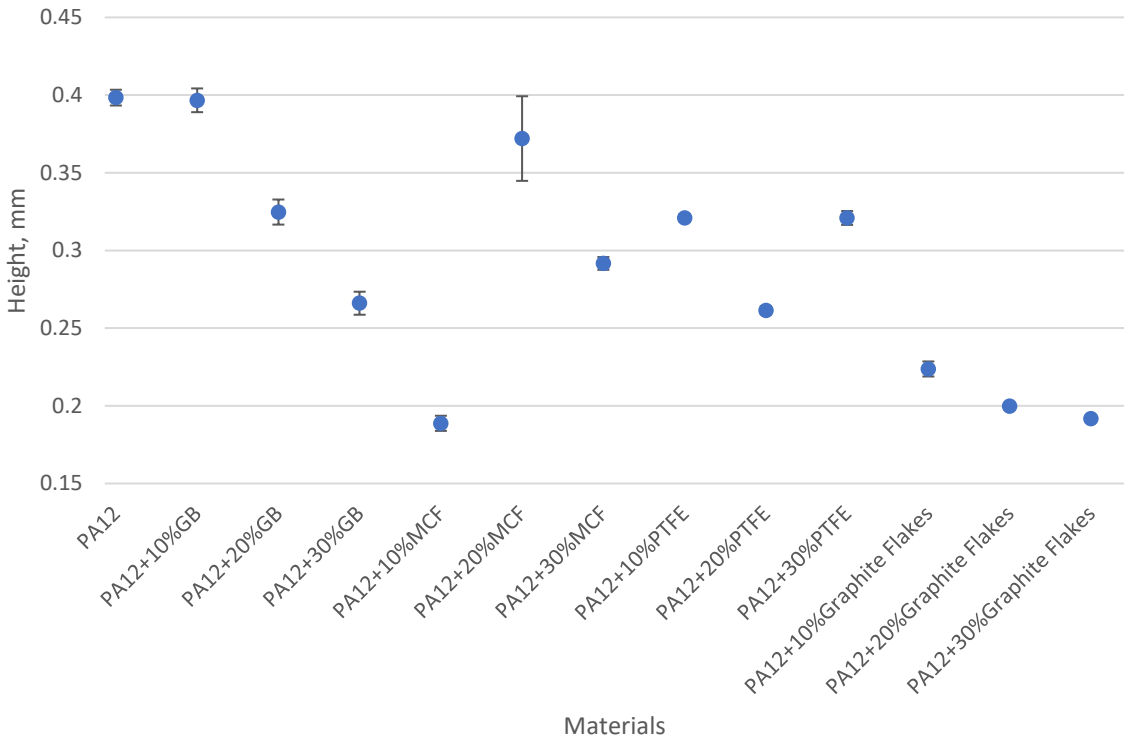

Figure 16 The average layer height determined for 3000mm/min speed bed movement for all PA12 combinations.

The addition of fillers can also have an effect on the overall weight of deposited powder. In most cases we can see higher concentration of fillers tends to produce lower weight of deposited material. This is due to the filler materials being lower in density compared with PA12. We can also observe that with PA12 combined with 20% milled carbon fibre we recorded a higher average layer thickness and deposited weight compared to lower concentrations of milled carbon fibre. This is due to the milled carbon fibre improving PA12 powder flow due to its fibrous structure that displaces and pushes more PA12 particles during agitation.

For PA12 combined with glass micro spheres, it was observed that the higher concentration of glass micro spheres resulted in heterogeneous deposition of powder. Formation of small stagnation points in the hopper were observed during deposition close to the nozzle, and this disruption of mass powder flow has effectively resulted in less material being ejected. The addition of PTFE, however, especially at 20%wt concentration, has been shown to improve mass flow from the hopper nozzle. The low surface energy of the PTFE powder in a way behaved as a powder flow enhancer, allowing more powder to be deposited through the nozzle. No pockets of stagnant flow or agglomeration was observed during the deposition trials for PA12 combined with 10, 20, or 30%wt concentration of PTFE.

6. Conclusion

The results presented in this paper illustrate a prototype design that could be utilised in the future to aid in the manufacture of multilayer, axially aligned filler composite materials. Present experimentation has highlighted the success of utilising a chisel shaped hopper design as a means of deposition of various powders and filler materials. Deposition trials, along with powder flow measurements, has aided in identifying what combinations of polyamide to filler

materials are beneficial for improved powder flow through the prototype, as well as determining what material combinations require further investigations. With powder flow rheology, we have determined that a maximum half angle of 43° is suitable to produce mass flow from our prototype design. Investigative research has supported our result and confirmed that a minimum half angle of 30° and a maximum of 70° can be used to achieve mass flow for powder materials with fairly regular spherical particles; however, more research is required to determine the optimum way of initiating alignment of fibrous fillers combined with polyamide.

The prototype designs that have been created for this research and that have been utilised in the deposition testing have provided a basis that can be used for further experimental testing. Recommendation for future work would be to test the prototype in a working PBF printer, along with exploring other design options presented in Figures 3 and 4.

Acknowledgements

The authors would like to gratefully acknowledge the generous financial support from the Engineering and Physical Sciences Research Council (EPSRC) UK and QinetiQ under the Prosperity Partnership Grant EP/N034627/1 for this research.

References

[1] Elsabbagh A, Ramzy A, Steuernagel L. et al. Models of flow behaviour and fibre distribution of injected moulded polypropylene reinforced with natural fibre composites. Composites Part B: Engineering. 2019;162:198-205.

[2] Ramzy A, El-Sabbagh A, Steuernagel L. et al. Rheology of natural fibers thermoplastic compounds: Flow length and fiber distribution. Journal of Applied Polymer Science. 2013;131(3).

[3] Peltola H, Madsen B, Joffe R. et al. Experimental Study of Fiber Length and Orientation in Injection Molded Natural Fiber/Starch Acetate Composites. Advances in Materials Science and Engineering. 2011;2011:1-7.

[4] Salman S, Leman Z, Sultan M. et al. The Effects of Orientation on the Mechanical and Morphological Properties of Woven Kenaf-reinforced Poly Vinyl Butyral Film. BioResources. 2015;11(1).

[5] Yang X, Yang W, Fan J. et al. Effects of molding on property of thermally conductive and electrically insulating polyamide 6–based composite. Journal of Thermoplastic Composite Materials. 2018;32(9):1190-1203.

[6] Zhou W, Qi S, Tu C. et al. Novel heat-conductive composite silicone rubber. Journal of Applied Polymer Science. 2007;104(4):2478-2483.

[7] Younesi, M. and Bahrololoom, M. Effect of temperature and pressure of hot pressing on the mechanical properties of PP–HA bio-composites. Materials & Design. 2009, 30(9): 3482-3488.

[8] Heckner, T., Seitz, M., Raisch, S., Huelder, G. and Middendorf, P., 2020. Selective Laser Sintering of PA6: Effect of Powder Recoating on Fibre Orientation. *Journal of Composites Science*, 4(3), p.108.

[9] Arai, S.; Tsunoda, S.; Yamaguchi, A.; Ougizawa, T. Effect of anisotropy in the build direction and laser-scanning conditions on characterization of short-glass-fiber-reinforced PBT for laser sintering. Opt. Laser Technol. 2019, 113, 345–356.

[10] Jansson, A. and Pejryd, L., 2016. Characterisation of carbon fibre-reinforced polyamide manufactured by selective laser sintering. *Additive Manufacturing*, 9, pp.7-13.

[11] Aerosint. 2021. *Selective Powder Deposition For Powder Bed Fusion 3D Printing - Aerosint*. [online] Available at: <https://aerosint.com/selective-powder-deposition/> [Accessed 11 January 2021].

[12] M. Binder, C. Anstaett, M. Horn, F. Herzer, G. Schlick, C. Seidel, J. Schilp, G. Reinhart, Potentials and challenges of multi-material processing by laser-based powder bed fusion, Texas, 2018. *(3) (PDF) Integration of Strain Gauges in Components Manufactured by Laser-BasedPowder Bed Fusion*. Available from: https://www.researchgate.net/publication/345867283_Integration_of_Strain_Gauges_in_Components_Manufactured_by_Laser-BasedPowder_Bed_Fusion [accessed Jan 11 2021].

[13] Beal, V. E., P. Erasenthiran, N. Hopkinson, P. Dickens and C. Ahrens. "Fabrication of x-graded H13 and Cu powder mix using high power pulsed Nd:YAG laser." (2004).

[14] Yardimci, A. M.; Guceri, S. I., Danforth, S. C. et al. Numerical Modeling of Fused Deposition Processing. Am. Soc. Mech. Eng. 1995; 69: 1225−1235.

[15] Rosenthal, M., Henneberger, C., Gutkes, A. et al. Liquid Deposition Modeling: a promising approach for 3D printing of wood. European Journal of Wood and Wood Products. 2017; 76(2): 797-799.

[16] Omar, N., Shuaib, N., Hadi, M. et al. Mechanical properties of carbon and glass fibre reinforced composites produced by additive manufacturing: A short review. IOP Conference Series: Materials Science and Engineering. 2019; 670(1): 012020.

[17] Tekinalp, H., Kunc, V., Velez-Garcia, G. et al. Highly oriented carbon fiber–polymer composites via additive manufacturing. Composites Science and Technology. 2014; 105: 144-150.

[18] Gardner, J., Sauti, G., Kim, J. et al. 3-D printing of multifunctional carbon nanotube yarn reinforced components. Additive Manufacturing. 2016; 12: 38-44.

[19] Christ, J., Aliheidari, N., Ameli, A. et al. 3D printed highly elastic strain sensors of multiwalled carbon nanotube/thermoplastic polyurethane nanocomposites. Materials & Design. 2017; 131: 394-401.

[20] Laureto J, Tomasi J, King J, et al. Thermal properties of 3-D printed polylactic acid-metal composites. Progress in Additive Manufacturing. 2017;2(1-2): 57-71.

[21] Masood S, Song W. Development of new metal/polymer materials for rapid tooling using Fused deposition modelling. Materials & Design. 2004;25(7): 587-594.

[22] Shulga E, Karamov R, S. Sergeichev I et al. Fused Filament Fabricated Polypropylene Composite Reinforced by Aligned Glass Fibers. Materials. 2020; 13(16): 3442.

[23] Hoque MJ, Chakraborty S, Mahbub M et al. Thermal conductivity of polypropylene based composite materials filled with graphite and carbon black. International Journal of Composite Materials. 2013; 3(5): 136-140.

[24] Pickering, K. and Stoof, D. Sustainable Composite Fused Deposition Modelling Filament Using Post-Consumer Recycled Polypropylene. Journal of Composites Science. 2017: 1(2): 17.

[25] Yang, C., Tian, X., Liu, T et al. 3D printing for continuous fiber reinforced thermoplastic composites: mechanism and performance. Rapid Prototyping Journal. 2017; 23(1): 209-215.

[26] Woern A, Byard D, Oakley R et al. Fused Particle Fabrication 3-D Printing: Recycled Materials' Optimization and Mechanical Properties. Materials. 2018;11(8):1413.

[27] Mohammed, M.I. Das, A. Gomez-kervin, E et al. EcoPrinting: Investigating the use of 100% recycled Acrylonitrile Butadiene Styrene (ABS) for Additive Manufacturing. In Proceedings of the 28th Annual International Solid Freeform Fabrication Symposium, Austin, TX, USA. 7–9 August 2017; 532–542.

[28] Farina I, Singh N, Colangelo F et al. High-Performance Nylon-6 Sustainable Filaments for Additive Manufacturing. Materials. 2019;12(23):3955.

[29] Valvez S, Santos P, Parente J et al. 3D printed continuous carbon fiber reinforced PLA composites: A short review. Procedia Structural Integrity. 2020;25:394-399.

[30] Goh G, Yap Y, Agarwala S et al. Recent Progress in Additive Manufacturing of Fiber Reinforced Polymer Composite. Advanced Materials Technologies. 2018;4(1):1800271.

[31]Dhakate S, Mathur R, Dhami T et al. Development of vapor grown carbon fibers (VGCF) reinforced carbon/carbon composites. Journal of Materials Science. 2006;41(13):4123-4131.

[32] Ning, F., Cong, W., Hu, Y et al. Additive manufacturing of carbon fiber-reinforced plastic composites using fused deposition modeling: Effects of process parameters on tensile properties. Journal of Composite Materials. 2016; 51(4):451-462.

[34] Shofner M, Lozano K, Rodríguez-Macías F et al. Nanofiber-reinforced polymers prepared by fused deposition modeling. Journal of Applied Polymer Science. 2003;89(11):3081-3090.

[35] L. J. Love, V. Kunc, O. Rios et al. The importance of carbon fiber to polymer additive manufacturing. Journal of Materials Research. 2014; 29(17): 1893-1898.

[36] Advances in carbon fiber 3D printing [Internet]. Reinforced Plastics. 2022 [cited 8 September 2022]. Available from: https://www.reinforcedplastics.com/content/products/advances-in-carbon-fiber-3d-printing.

[37] Invernizzi M, Natale G, Levi M et al. UV-Assisted 3D Printing of Glass and Carbon Fiber-Reinforced Dual-Cure Polymer Composites. Materials. 2016;9(7):583.

[38] Compton B, Lewis J. 3D Printing: 3D-Printing of Lightweight Cellular Composites (Adv. Mater. 34/2014). Advanced Materials. 2014;26(34):6043-6043.

[39] Postiglione G, Natale G, Griffini G et al. Conductive 3D microstructures by direct 3D printing of polymer/carbon nanotube nanocomposites via liquid deposition modeling. Composites Part A: Applied Science and Manufacturing. 2015;76:110-114.

[40] Roh S, Choi E, Choi Y et al. Characterization of the surface energies of functionalized multi-walled carbon nanotubes and their interfacial adhesion energies with various polymers. Polymer. 2014;55(6):1527-1536.

[41] Kim J, Lee S, Wajahat M et al. Three-Dimensional Printing of Highly Conductive Carbon Nanotube Microarchitectures with Fluid Ink. ACS Nano. 2016;10(9):8879-8887.

[42] Mora A, Verma P, Kumar S. Electrical conductivity of CNT/polymer composites: 3D printing, measurements and modeling. Composites Part B: Engineering. 2020;183:107600.

[43] Raney J, Compton B, Mueller J et al. Rotational 3D printing of damage-tolerant composites with programmable mechanics. Proceedings of the National Academy of Sciences. 2018;115(6):1198-1203.

[44] Abu Bakar Sulong, Park J. Alignment of multi-walled carbon nanotubes in a polyethylene matrix by extrusion shear flow: mechanical properties enhancement. Journal of Composite Materials. 2010;45(8):931-941.

[45] Gherardini L, Cousins C, Hawkes J et al. A new immobilisation method to arrange particles in a gel matrix by ultrasound standing waves. Ultrasound in Medicine & Biology. 2005;31(2):261-272.

[46] Kim G, Shkel Y. Analysis of the electro-orientation of inorganic micro/nano-particles in a liquid polymer considering electrophoresis flow. Journal of Micromechanics and Microengineering. 2007;17(12):2522-2527.

[47] Cao Y, Xie W, Sun J et al. Preparation of epoxy blends with nanoparticles by acoustic levitation technique. Journal of Applied Polymer Science. 2002;86(1):84-89.

[48] Saito M, Daian T, Hayashi K et al. Fabrication of a polymer composite with periodic structure by the use of ultrasonic waves. Journal of Applied Physics. 1998;83(7):3490-3494.

[49] Llewellyn-Jones T, Drinkwater B, Trask R. 3D printed components with ultrasonically arranged microscale structure. Smart Materials and Structures. 2016;25(2):02LT01.

[50] Glynne-Jones P, Boltryk R, Harris N. et al. Mode-switching: A new technique for electronically varying the agglomeration position in an acoustic particle manipulator. Ultrasonics. 2010;50(1):68-75.

[51] Wu J, Du G. Acoustic radiation force on a small compressible sphere in a focused beam. The Journal of the Acoustical Society of America. 1990;87(3):997-1003.

[52] Glynne-Jones P, Demore C. et al. Array-controlled ultrasonic manipulation of particles in planar acoustic resonator. IEEE Transactions on Ultrasonics, Ferroelectrics and Frequency Control. 2012;59(6):1258-1266.

[53] Scholz M, Drinkwater B, Trask R. Ultrasonic assembly of anisotropic short fibre reinforced composites. Ultrasonics. 2014;54(4):1015-1019.

[54] T. Kozuka, T. Tuziuti, H. Mitome, et al. Acoustic micromanipulation usinga multi-electrode transducer, in: Proceedings of the Seventh International Symposium on Micro Machine and Human Science. 1996; 163–170.

[55] Courtney C, Ong C, Drinkwater B. et al. Manipulation of particles in two dimensions using phase controllable ultrasonic standing waves. Proceedings of the Royal Society A: Mathematical, Physical and Engineering Sciences. 2011;468(2138):337-360.

[56] Yunus D, Sohrabi S, He R. Acoustic patterning for 3D embedded electrically conductive wire in stereolithography. Journal of Micromechanics and Microengineering. 2017;27(4):045016.

[57] Collino R, Ray T, Friedrich L. et al. Scaling relationships for acoustic control of two-phase microstructures during direct-write printing. Materials Research Letters. 2018;6(3):191-198.

[58] Hopper Design Principles - Chemical Engineering [Internet]. Chemical Engineering. 2022 [cited 8 September 2022]. Available from: https://www.chemengonline.com/hopper-design-principles/

[59] New FT4 Powder Rheometer Software [Internet]. Freemantech.co.uk. 2022 [cited 4 May 2022]. Available from: https://www.freemantech.co.uk/news/new-software-for-freeman-technology-ft4-simplifies-hopper-design.

[60] Products [Internet]. Gunt.de. 2022 [cited 14 January 2022]. Available from: https://www.gunt.de/en/products/process-engineering/mechanical-process-engineering/storage-and-flow-of-bulk-solids/flow-of-bulk-solids-from-silos/083.21000/ce210/glct-1:pa-148:ca-237:pr-14.

[61] Teflon.com. 2022. [online] Available at: <https://www.teflon.com/en/-/media/files/teflon/zonyl-mp-1100-product-info.pdf?rev=d888aa649a4a4f58a8223063705345fe&hash=3557D68DBE5F0A0A6CB10D8CCE428F0B> [Accessed 7 September 2022].

[62] Sigmaaldrich.com. 2022. [online] Available at: <https://www.sigmaaldrich.com/GB/en/sds/aldrich/440345> [Accessed 7 September 2022].

[63] Sigmaaldrich.com. 2022. [online] Available at: <https://www.sigmaaldrich.com/GB/en/sds/aldrich/332461> [Accessed 7 September 2022].

[64] Media.easycomposites.co.uk. 2022. [online] Available at: <https://media.easycomposites.co.uk/datasheets/EC-SDS-Carbiso-Milled-Carbon-Fibre.pdf> [Accessed 7 September 2022].

[65] Chung H, Das S. Processing and properties of glass bead particulate-filled functionally graded Nylon-11 composites produced by selective laser sintering. Materials Science and Engineering: A. 2006; 437(2): 226-234.

[66] Mehos, G. and Morgan, D., 2016. *Hopper Design Principles - Chemical Engineering*. [online] Chemengonline.com. Available at: <https://www.chemengonline.com/hopper-design-principles/?printmode=1> [Accessed 17 May 2020].

[67] Gunt.de. 2021. *Products*. [online] Available at: <https://www.gunt.de/en/products/process-engineering/mechanical-process-engineering/storage-and-flow-of-bulk-solids/flow-of-bulk-solids-from-silos/083.21000/ce210/glct-1:pa-148:ca-237:pr-14> [Accessed 14 January 2021].